Weierstraß-Institut

für Angewandte Analysis und Stochastik

Leibniz-Institut im Forschungsverbund Berlin e. V.

Preprint ISSN 2198-5855

Numerics of thin-film free boundary problems for partial wetting

Dirk Peschka

submitted: October 2, 2014

Weierstrass Institute
Mohrenstraße 39
10117 Berlin
Germany

No. 2016

Berlin 2014

2000 *Mathematics Subject Classification.* 76A20, 35R35, 76M10.

Key words and phrases. thin films, free boundary problems, numerics.

Financial support by DFG Research Center MATHEON (C10).

Edited by
Weierstraß-Institut für Angewandte Analysis und Stochastik (WIAS)
Leibniz-Institut im Forschungsverbund Berlin e. V.
Mohrenstraße 39
10117 Berlin
Germany

Fax: +49 30 20372-303
E-Mail: preprint@wias-berlin.de
World Wide Web: http://www.wias-berlin.de/

Abstract

We present a novel framework to solve thin-film equations with an explicit non-zero contact angle, where the support of the solution is treated as an unknown. The algorithm uses a finite element method based on a gradient formulation of the thin-film equations coupled to an arbitrary Lagrangian-Eulerian method for the motion of the support. Features of this algorithm are its simplicity and robustness. We apply this algorithm in 1D and 2D to problems with surface tension, contact angles and with gravity.

1 Introduction and model statement

In this paper we describe the creeping motion of a viscous liquid over a flat solid substrate. If we assume that at each time t the liquid occupies the volume

$$\Omega(t) = \{(x, y, z) \in \mathbb{R}^3 : 0 < z < h(t, x, y)\},$$

then the interface between the liquid and the surrounding air is located at $z = h(t, x, y)$ and the solid substrate is at $z = 0$. The shape of the liquid domain can be entirely parametrized by the function $h(t, x, y)$. In the thin-film limit of the Stokes equation, the evolution of the $\Omega(t)$ is given by solving

$$\partial_t h = \nabla \cdot (m(h)\nabla\pi), \tag{1.1}$$

with given initial data $h(0, x, y) = h_0(x, y) \geq 0$. The mobility m is a nonnegative, monotone function with $m(0) = 0$ and typically one has power-laws $m(h) = h^\alpha$ with $0 < \alpha \leq 3$ depending on the type of friction at the substrate [1]. The most studied case is certainly the no-slip boundary condition with $\alpha = 3$, see [2] and references therein. To avoid a singular energy dissipation [3, 4] a slip condition with $\alpha = 2$ was proposed. The case $\alpha = 1$ is relevant for liquid motion on a porous rough surfaces or in Hele-Shaw cells [5, 6]. The evolution is driven by an energy

$$E(h) = \int_{\mathbb{R}^2} \frac{1}{2}|\nabla h|^2 \mathrm{d}x\,\mathrm{d}y + V(h), \tag{1.2}$$

and the pressure in (1.1) is defined $\pi = \delta E/\delta h$. What makes this problem sometimes difficult to treat analytically and numerically is the fact, that the function h may vanish in certain regions and thereby the support of h

$$\omega(t) = \big\{(x, y) \in \mathbb{R}^2 : h(t, x, y) > 0\big\}, \tag{1.3}$$

depends on time. This makes the partial differential equation a free boundary problem. Depending on $V(h)$ there are different strategies to tackle this difficulty.

For $V \equiv 0$ we are in the situation where the liquid spreads over the substrate with zero contact angle. Algorithms were constructed which use a globally defined $h(t,\cdot)$ and enjoy the property of maintaining positivity or non-negativity [7–9]. This is based on the observation by Bernis & Friedmann [10] that the thin film equation has, in addition to its energy dissipation

$$\tfrac{d}{dt}E(h) = -\int m(\nabla\pi)^2 \,\mathrm{d}x\,\mathrm{d}y \leq\ 0,$$

also a nonlinear entropy dissipation $\partial_t \int G(h) = -\int(\Delta h)^2$. In addition to a entropy-based discretization it might be necessary to regularize the mobility to ensure non-negativity. This class of algorithms is certainly computationally efficient, since the computational domain is fixed. Thereby people can apply highly developed numerical methods and obtain beautiful numerical results. For a review concerning the mathematics of the contact line problem we recommend the short review by Bertozzi [11]. In order to treat finite contact angles intermolecular potentials such as

$$V(h) = \int_{\mathbb{R}^2} \left(\frac{A}{h^2} - \frac{B}{h^8}\right) \mathrm{d}x\,\mathrm{d}y, \tag{1.4}$$

were introduced, e.g. [12, 13] or [2] and references therein. For numerical results in 2D with heterogeneous substrates we refer to [14]. Such a choice might ensure even global positivity of h and produce contact angles in a certain sense. Compared to the case $V \equiv 0$ these methods are still quite easy to implement but usually require spatial adaptivity near the approximate contact line. This makes the algorithms potentially sluggish in higher dimensions. The big advantage of these methods is that there is no problem with changes in topology, i.e. when connectivity properties of ω change.

The main reason for the simplicity and success of these methods might be that one actually never has to deal with a free boundary problem at all. In this paper we pursue an entirely different strategy. The intent of this paper is to consider the case of non-smooth V such as

$$V(h) = S\int_{\mathbb{R}^2} \chi_\omega \,\mathrm{d}x\,\mathrm{d}y, \tag{1.5}$$

which measures the size of the support (wetted region) using the characteristic function χ_ω of the support ω

$$\chi_\omega = \begin{cases} 1 & (x,y) \in \omega \\ 0 & \text{otherwise} \end{cases},$$

and the parameter $S \geq 0$ is the negative spreading coefficient for partial wetting. This is interesting because for $S = 0$ we cover the case $V \equiv 0$ and for $S > 0$ we use a V which is a limiting case of the intermolecular potential in (1.4) as was shown in [15]. We solve this as a free boundary problem, where the support ω in (1.3) is one of the unknowns. Our strategy is to solve a variational formulation to obtain $\partial_t h$ and then

For the case $V \equiv 0$ short-time existence and uniqueness of *classical* solutions was proven by Giacomelli & Knüpfer [16] also in the context of a moving support, which is in contrast to

the conventional approach using the concept of weak solutions by Bernis & Friedman[10]. The contact line singularity for an explicit contact line has been investigated by Flitton & King [17] using formal asymptotics and by Giacomelli et al. [18] rigorously.

From a numerical standpoint the present work is somewhat similar to the one by Karapetsas et al. [19] but without surfactants. The main differences are that we evaluate local conditions in a gradient-type formulation. So all boundary conditions follow naturally from the variational formulation. Due to the locality we can easily generalize this algorithm to higher dimensions. A similar but technically more involved derivation of a gradient formulation for bilayer films was given in [20]. The inherent disadvantage of such a method is that it can not handle topological changes of the support. Still we want to convince the reader that, with a little knowledge of finite elements, such a formulation can be superior to the classical approaches.

2 Numerical algorithm

2.1 Weak formulation

We assume h is a globally continuous function with continuous first derivatives inside ω. Furthermore we assume that the support ω moves with finite speed. Then the main idea of the algorithm is to solve (1.1) only inside ω with additional boundary conditions and kinematic conditions at the boundary $\gamma = \partial\omega$. The kinematic condition is implied by the fact that $h = 0$ on γ. In order to solve (1.1) on ω we construct a variation formulation of the thin-film equation. Therefore we integrate (1.1) by parts and use the fact that the flux $m\nabla\pi$ is zero on γ. Then we get

$$\int_\omega \big(\partial_t h\,\phi\ + m(h)\nabla\pi\cdot\nabla\phi\,\big)\,\mathrm{d}x\,\mathrm{d}y = 0. \tag{2.1}$$

In order to see how to define π in this weak formulation, let us carefully compute the derivative of

$$E(h) = \int_{\mathbb{R}^2}\left(\frac{1}{2}|\nabla h|^2 + S\chi_\omega\right)\mathrm{d}x\,\mathrm{d}y,$$

at least in a formal sense. Using Reynolds' transport theorem we get

$$\begin{aligned}\frac{d}{dt}E &= \int_\omega \nabla h\cdot\nabla\dot{h}\,\mathrm{d}\omega + \int_\gamma \big(S+\tfrac{1}{2}|\nabla h|^2\big)\,\dot{\mathbf{x}}\cdot\mathbf{n}\,\mathrm{d}\gamma,\\ &= \int_\omega \nabla h\cdot\nabla\dot{h}\,\mathrm{d}\omega - \int_\gamma |\nabla h|^{-1}\,\big(S+\tfrac{1}{2}|\nabla h|^2\big)\,\dot{h}\,\mathrm{d}\gamma,\end{aligned} \tag{2.2}$$

where $\dot{h} = \partial_t h$ and $\dot{\mathbf{x}}\cdot\mathbf{n}$ is the normal component of the velocity of the boundary γ. To get to the last line we used our assumption that $h \equiv 0$ on γ. Differentiating this with respect to time we get

$$\dot{h} + \dot{\mathbf{x}}\cdot\nabla h = 0, \qquad \text{on } \gamma, \tag{2.3}$$

which using $\mathbf{n} = \nabla h/|\nabla h|$ gives (2.2). So setting $\pi = \delta E/\delta h$ in a weak sense on ω means $\langle \pi, \psi \rangle = dE[\psi]$ and thereby

$$\int_\omega \pi\psi \,\mathrm{d}\omega = \int_\omega \nabla h \cdot \nabla\psi \,\mathrm{d}\omega - \int_\gamma |\nabla h|^{-1} \left(S + \tfrac{1}{2}|\nabla h|^2\right) \psi \,\mathrm{d}\gamma. \tag{2.4}$$

Finally we seek $(\dot{h}, \pi)$ by solving (2.1) together with (2.4) as our weak formulation. All boundary conditions here are natural boundary conditions, time derivatives $\dot{h}$ are understood as in the Eulerian reference frame.

2.2 Kinematic condition

Now assume that we already know the solution $h(t, x, y)$ and have computed the corresponding $\dot{h}$ inside ω. For the time-discretization the remaining question is how to compute $h(t + \tau, x, y)$ and $\omega(t + \tau)$. Setting $h(t + \tau, \cdot, \cdot) = h(t, \cdot, \cdot) + \tau\dot{h}$ makes no sense since $h(t + \tau, \cdot, \cdot)$ and $h(t, \cdot, \cdot)$ are defined on different domains. Instead we use (2.3) and define an interpolation $\dot{\psi}$ of $\dot{\mathbf{x}}$ into the interior and make that depend on time. Obviously $\dot{\psi}$ should satisfy $\dot{\psi} = \dot{\mathbf{x}}$ on γ. Then from $\omega(t)$ we can consistently define $\omega(t + \tau)$ using $x + \tau\dot{\psi} \in \omega(t + \tau)$ for all points $x \in \omega(t)$. Note that (2.3) only defines the normal component of $\dot{\mathbf{x}}$, so one can freely choose the tangential component. In order to simplify things here, we first consider the 1D case, which we can understand as the situation with translational invariance in y direction, i.e. $h(t, x) = h(t, x, y)$ for all y.

1-dimensional case

The case is treated separately, because we can define the interpolation explicitly. This makes the construction easier and more comprehensible. Assume we have $\omega(t) = (x_-(t), x_+(t))$ being a single interval, correspondingly we know $\dot{x}_\pm$. Now define

$$\dot{\psi}(x) = (\dot{x}_+ - \dot{x}_-)\xi(x) + \dot{x}_-, \tag{2.5}$$

where $\xi(x) = (x - x_-)/(x_+ - x_-)$. The values of $\dot{x}_\pm$ we get from (2.3) using $\dot{h}$ and ∇h on γ. If we are going to move the domain according to $\dot{\psi}$, then we should change the time-derivative accordingly. If we define $H(t, x) = h(t, \psi(x))$, then $\dot{H} = \dot{h} + \dot{\psi} \cdot \nabla h$. Then condition (2.3) implies that in a comoving frame $\dot{H} = 0$, i.e. $H \equiv 0$. If $\dot{h}$ is known, then we can use ∇h to decompose it into $\dot{\psi}$ and $\dot{H}$. Once the interpolation is defined, this decomposition is unique.

higher-dimensional case

The 1-dimensional case is quite generic in the choice of the interpolation, whereas the optimal choice in the higher-dimensional situation depends much on the behavior of the solution. Let us first consider an interpolation, where $\dot{\psi}$ has no tangential component on γ. One possible choice would be

$$\dot{\psi} = \alpha \nabla h,$$

where α is a yet-to-be-determined function. Using the conditions above we get

$$\alpha = -\frac{\dot{h}}{|\nabla h|^2},$$

on γ. Since $\dot{\psi}$ is uniquely defined by α and we have its boundary data, we can interpolate $\dot{\psi}$ by defining α as harmonic. In general the choice of the interpolation and the tangential direction of $\dot{\psi}$ is entirely arbitrary and driven by computational simplicity. In one example of the next section we show, how the tangential part of $\dot{\psi}$ can be modified to obtain a more robust deformation.

2.3 Algorithm summarized

Let us summarize the algorithm, given the solution $h(t,\cdot)$ at an arbitrary time t with support $\omega(t)$.

1 First compute the time derivative $\dot{h} \in V_h$ by solving the weak formulation

$$\begin{aligned}\int_\omega \big(\dot{h}\,\phi \; + m(h)\nabla\pi\cdot\nabla\phi\big)\,\mathrm{d}\omega &= 0\\ \int_\omega \pi\psi\,\mathrm{d}\omega = \int_\omega \nabla h\cdot\nabla\psi\,\mathrm{d}\omega &- \int_\gamma |\nabla h|^{-1}\left(S+\tfrac{1}{2}|\nabla h|^2\right)\psi\,\mathrm{d}\gamma,\end{aligned}$$

for all $\psi,\phi \in V_h$ from a suitable discrete function space V_h. Note this will produce the proper contact angle, since the boundary term from the derivative $\delta E/\delta h$ is included here. In the actual numerical scheme a semi-implicit time-discretization is desirable for stability reasons. This can be done by replacing h in the first integral on the right side of the second equation by $h+\tau\dot{h}$. In this paper we choose V_h in the Galerkin approximation as piecewise linear polynomials on intervals (1D) or triangles (2D). None of these spaces of functions has any restrictions due to essential boundary conditions.

2 Based on the knowledge of the normal part of the velocity $\dot{\mathbf{x}}$ and after a possible modification of the tangential part one defines an interpolation $\dot{\psi}$ to the inside. In one dimension this can be by defining

$$\dot{\psi}(x) = (\dot{x}_+ - \dot{x}_-)\xi(x) + \dot{x}_-,$$

with ξ as defined before. The choice for the tangential part and for the interpolation depends very much on the problem at hand. For instance, if one wants to find traveling wave solutions (in higher dimensions) then one could choose the tangential part such that $\dot{\psi}$ might be constant in space.

3 As soon as the choice for $\dot{\psi}$ has been made, chain rule gives

$$\dot{H} = \dot{h} + \dot{\psi}\cdot\nabla h,$$

which defines the time-derivative in a Lagrangian system $\dot{H}$. Now we move all the vertices of the domain $\mathbf{x} \mapsto \mathbf{x} + \tau\dot{\psi}$ and all the nodal values $h \mapsto h + \tau\dot{H}$ to obtain the new solution at time $t+\tau$.

The first step of the algorithm is rather standard, but to our knowledge was not applied to a free-boundary problem of thin-film type. In particular it was not used in combination with our decomposition of the time-derivative into the transport velocity $\dot{\psi}$ and the time derivative $\dot{H}$ in the corresponding comoving frame. In the work by Karapetsas et al. [21] the velocity/position of the contact-line is determined from the global mass conservation constraint. However, since this is only one scalar constraint such an approach only works in one spatial dimension with a single contact point. Karapetsas et al. argued that the evaluation of the usual kinematic conditions $\dot{\mathbf{x}} = (m/h)\nabla\Delta h$ is not feasible, since it contains the product of the singular term $\nabla\Delta h$ and the degenerate term m/h as one approaches the boundary. It is certainly unclear how to design a robust algorithm which takes this condition literally. In this sense our approach has the advantage that we only work with $\dot{h}, \nabla h$, both of which are neither degenerate nor singular at the contact line. In addition we use local conditions, which make it possible to extend the algorithm to higher dimensions. To underline this claim we present some examples in 1D and 2D.

3 Examples in 1D

Here we consider an extension of the energy considered before, namely

$$V(h) = \int_\omega S + f(h; x)\,\mathrm{d}\omega\,, \tag{3.1}$$

where f may explicitly depend on x in a parametric way. Thereby we can include effects such as partial wetting and gravity in x (tangential) and z (normal) direction. Without the tangential component we get stationary solutions, whereas with a tangential component of gravity and sufficiently small volumes we get stable traveling wave solutions. The numerical solution of the algorithm above with $m(h) = h^2$, $f \equiv 0$, $S = 1$, $L = 1$ with initial data $h_0(x) = L/2 - |x - L/2|$ is shown in fig. 1. Note that we choose the mobility with this exponent to circumvent the certainly interesting discussion on the contact line singularity, which would prevent any motion of the contact line.

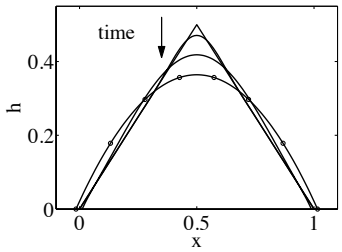

Figure 1: Evolution towards a stationary droplet at $t = 10^{-5}, t = 10^{-3}, t = 10$ as indicated by the arrow.

The energy above implies the contact angle is $|\partial_x h| = \sqrt{2}$ at $x_\pm$ and the stationary solution is

$$h(x) = \frac{\alpha}{\sqrt{2}}\left(1 - \left(\frac{x - 1/2}{\alpha}\right)^2\right),$$

where $x \in (1/2 - \alpha, 1/2 + \alpha)$ and $\alpha^2 = \sqrt{18}/16$. In fig. 1 the exact solution is shown using a few points overlaying the numerical solution with full lines. Already at $t = 10$ there is no visible change in the solution and the comparison with the exact stationary solution is very good. The simulation shown here was performed using $n = 100$ elements and a nonuniform time-step size. Even though the initial data provided here is not continuously differentiable at $x = 1/2$, the numerical algorithm had no problems finding the stationary state on coarse or on fine meshes with $n = 100$ or $n = 1000$ elements and big time-step sizes such as $\tau = 10^3$. In this sense the algorithm might be also suited just to find stationary solutions of this type of PDE problems.

Gravity in tangential direction can be included in the problem by using $f(h; x) = -g_1 x h$, where g_1 encodes the strength of gravitational forces. Here we use $g_1 = 1$. Then the total energy of the system can be decreased by moving the droplet in $+x$ direction. The corresponding PDE solution is shown in fig. 2 for the same initial data as before but with $L = 1$ (left panel) and $L = 5$ (right panel). The traveling wave solution for the bigger volume is more asymmetric.

The quasi stationary traveling wave solutions with sharp contact angles have been studied in some detail by Kriegsmann & Miksis [22]. At that time the numerical treatment of the dynamical sharp interface problem was unclear. Nevertheless they performed an ODE analysis of quasi stationary traveling wave solutions.

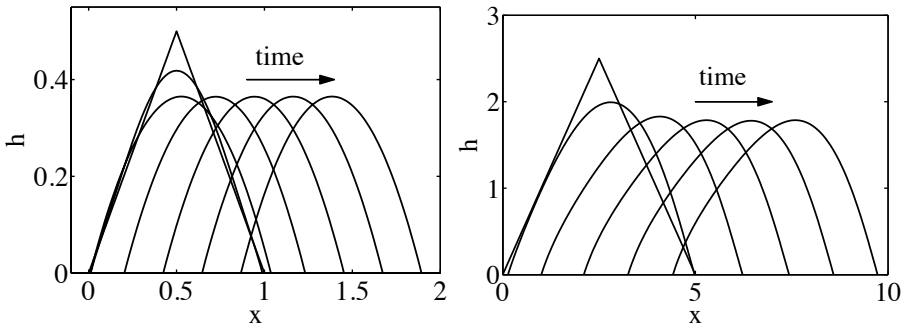

Figure 2: Evolution towards a traveling wave solution under the action of gravitational forces in tangential direction for small volumes $L = 1$ at $t = (0, 10^{-3}, 0.1, 1, 2, 3, 4)$ (left) and bigger volumes $L = 5$ and $t = (0, 0.1, 1, 2, 3, 4)$ (right).

The third and rather simple example is to add normal gravitational forces, which can be achieved by using for instance $f(h; x) = g_2 h^2$, where g_2 encodes the strength of normal gravitation forces. Here we use $g_2 = 10^2$. Then the total energy of the system can be decreased by making the droplet from fig. 1 slightly flat, as one can observe in fig. 3

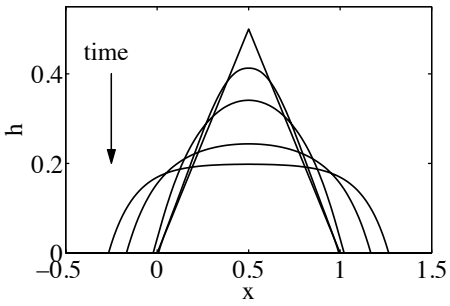

Figure 3: Evolution towards a stationary droplet under normal gravitational forces at $t = (0, 10^{-3}, 0.01, 0.1, 1)/2$ as indicated by the arrow.

4 Examples in 2D

Similar to the 1D example we use the extended potential (3.1) with

$$f(h; x) = -g_1 hx + g_2 h^2$$

where we use f again to implement gravitation in the tangential and normal direction using g_1 and g_2 respectively. In the first example in fig. 4 we use an initial flower shaped domain, where the boundary in polar coordinates is at $r(\phi) = 5(1 + \sin 3\phi)$. The initial height solves $-\Delta h_0 = 1$ with homogeneous Dirichlet boundary conditions. Here we use $S = 2, g_1 = g_2 = 0$ which gives rise to a contact angle $|\nabla h| = 2$ at γ. As expected, the evolution depicted in fig. 4 is headed toward the stationary droplet state, i.e. a parabola which is cut-off at $h = 0$ and the proper contact angle and volume. Degradation of mesh quality during the evolution was handeled using remeshing and interpolating the previous solution in the new mesh by linear interpolation. In this case this was the most severe source of loss of mass. This can be avoided if one chooses an interpolation which maintains a good mesh quality for a longer time (or by improving the interpolation of course).

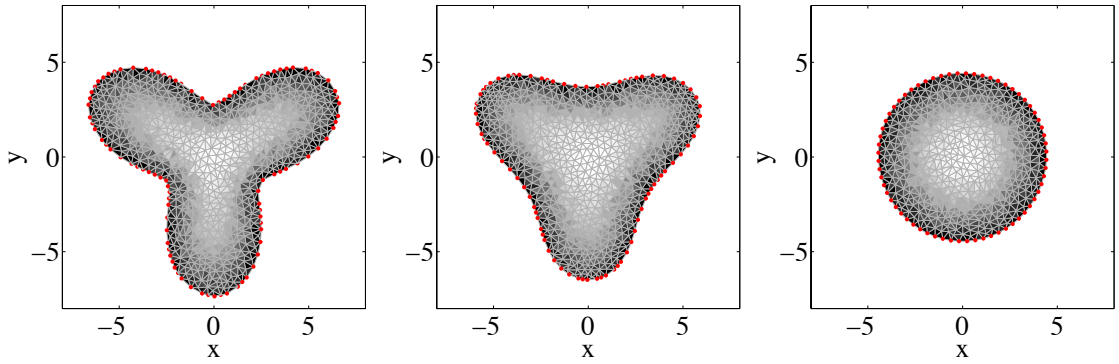

Figure 4: Evolution towards stationary droplet at $t = 0,\ 3,\ 12$ (left) to (right) where height is indicated by the shading

The next example shows how we can maintain mesh quality in certain situations somewhat

longer. This example uses an initial disc of radius $r = 5$ and a parabola for $h_0(x, y)$. As a driving force we use gravity with $g_1 = 0.2$ and $g_2 = 1$. As in the 1D case this should result in a traveling wave solution, i.e. a droplet moving in $+x$ direction. That this is clearly the case, can be seen in the panels of fig. 5. Quite from the beginning the velocity is mainly a translation with velocity v in x direction. However, in the simulation in the middle panel of this figure we only use the normal component to move the domain. In order to find out what this implies let us for a moment assume that the domain is still a ball of radius r. Then for points on the boundary we get in a comoving frame

$$\dot{\psi} - \begin{pmatrix} v \\ 0 \end{pmatrix} = v \frac{x}{x^2 + y^2} \begin{pmatrix} x \\ y \end{pmatrix} - \begin{pmatrix} v \\ 0 \end{pmatrix} = \frac{v}{x^2 + y^2} \begin{pmatrix} -y^2 \\ xy \end{pmatrix},$$

so there is the clear tendency to transport points from the front of the droplet to its back. This is exactly what happens in the middle panel of fig. 5. In order to prevent this effect, we choose the tangential part of $\dot{\psi}$ more carefully. In particular we want this method to work with traveling wave solutions. We do this by finding $(v_x, v_y) \in \mathbb{R}^2$, so that

$$\int_\gamma \Big(\big((v_x, v_y)^\top - \dot{x} \big) \cdot \mathbf{n} \Big)^2 \mathrm{d}\gamma,$$

is minimal. The remaining part we choose so that $\dot{\psi} = (v_x, v_y)^\top + \alpha \nabla h$ where the boundary values for α are chosen accordingly and α is harmonic inside ω. The resulting deformation at $t = 14$ is shown in the right panel of fig. 5. This result is obtained without using any remeshing.

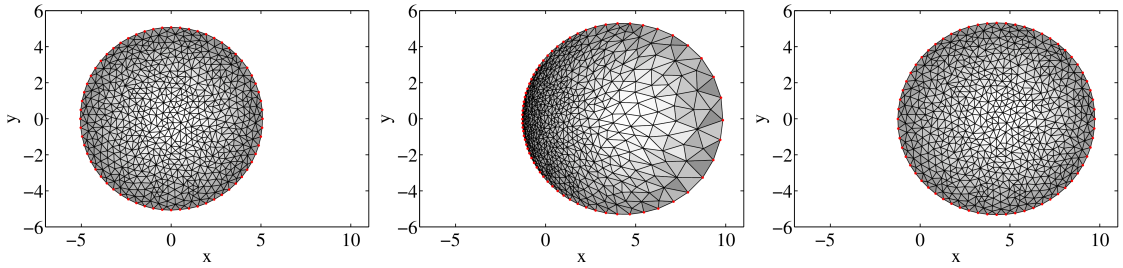

Figure 5: Droplet under the action of gravity at $t = 0$ (left) and at $t = 14$ (middle, right). Comparison between choice of the tangential component (middle) none (right) optimal constant (ν_x, ν_y).

With stronger gravity g_1 the droplet shape again becomes more asymmetric in time and real droplets would eventually decay into smaller satellite droplets after some finite time. This can be seen in fig. 6, where we combine the optimized transport with remeshing every 50 time-steps. For the largest value $g_1 = 0.8$ the final solution h is close to a pinch-off.

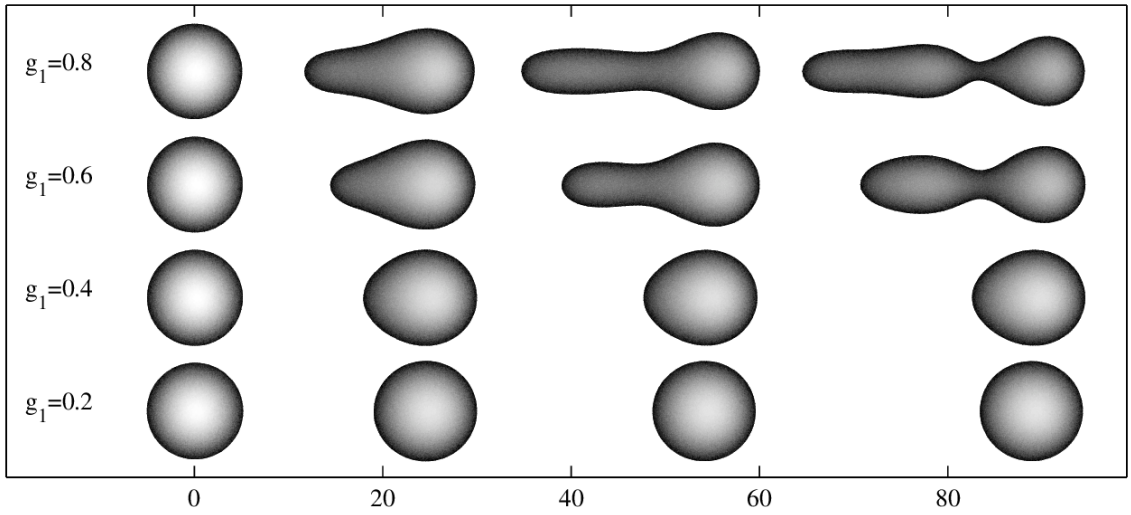

Figure 6: motion of droplets due to gravitational force $g_2 = 1$ and different g_1 at increasing times (left to right)

A similar investigation can also be done with the mobility $m(h) = \frac{1}{3}h^3 + 0.1h^2$, where the quadratic term is included in order to prevent problems due to the infinite dissipation of a moving contact line for $\alpha = 3$. We basically observe the same instability mechanism, i.e. at sufficiently large tangential gravitational forces g_1 satellite droplets pinch off. Compared to the case $\alpha = 2$ this happens already at smaller values of g_1. A systematic study of possible droplet shapes for different values of g_1, g_2 and comparison with experiments as in [23] are interesting questions for future studies.

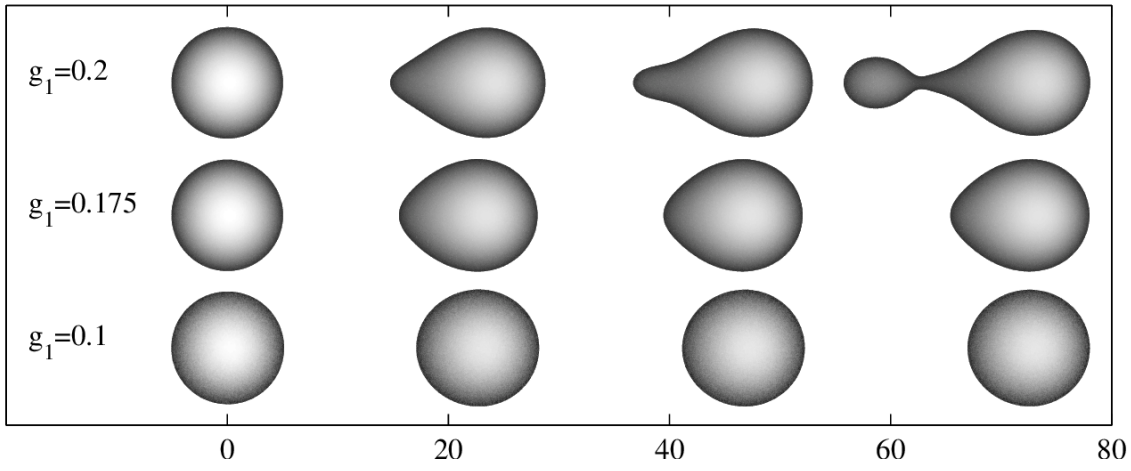

Figure 7: motion of droplets due to gravitational force as in fig. 6 but with $m(h) = \frac{1}{3}h^3 + 0.1h^2$

5 Conclusion

We showed that the thin-film free boundary problem can be efficiently solved in 1D and 2D with an explicit contact line. Therefore we employ a gradient-type finite element method, together with a simple method to employ a kinematic condition. We showed that sometimes one can use the ambiguity in the tangential component of $\dot{\psi}$ to obtain a mesh update, by which the mesh quality does not degrade too quick.

Acknowledgement

I am thankful for many fruitful discussions with Robert Huth, with whom I started to discuss different ways to tackle this problem. The extension of this work to liquid bilayers is joint work with Sebastian Jachalski and Georgy Kitavtsev, who I wish to thank as well. The financial support by the Research Center MATHEON is kindly acknowledged.

References

[1] J. Eggers, Toward a description of contact line motion at higher capillary numbers, Physics of Fluids (1994-present) 16 (9) (2004) 3491–3494.

[2] A. Oron, S. H. Davis, S. G. Bankoff, Long-scale evolution of thin liquid films, Reviews of Modern Physics 69 (3) (1997) 931.

[3] C. Huh, L. Scriven, Hydrodynamic model of steady movement of a solid/liquid/fluid contact line, Journal of Colloid and Interface Science 35 (1) (1971) 85–101.

[4] L. Hocking, Sliding and spreading of thin two-dimensional drops, The Quarterly Journal of Mechanics and Applied Mathematics 34 (1) (1981) 37–55.

[5] P. Neogi, C. A. Miller, Spreading kinetics of a drop on a rough solid surface, Journal of Colloid and Interface Science 92 (2) (1983) 338–349.

[6] P. Constantin, T. F. Dupont, R. E. Goldstein, L. P. Kadanoff, M. J. Shelley, S.-M. Zhou, Droplet breakup in a model of the hele-shaw cell, Physical Review E 47 (6) (1993) 4169.

[7] L. Zhornitskaya, A. L. Bertozzi, Positivity-preserving numerical schemes for lubrication-type equations, SIAM Journal on Numerical Analysis 37 (2) (1999) 523–555.

[8] G. Grün, M. Rumpf, Nonnegativity preserving convergent schemes for the thin film equation, Numerische Mathematik 87 (1) (2000) 113–152.

[9] J. A. Diez, L. Kondic, Computing three-dimensional thin film flows including contact lines, Journal of Computational Physics 183 (1) (2002) 274–306.

[10] F. Bernis, A. Friedman, Higher order nonlinear degenerate parabolic equations, Journal of Differential Equations 83 (1) (1990) 179–206.

[11] A. L. Bertozzi, The mathematics of moving contact lines in thin liquid films, Notices AMS 45 (1998) 689–697.

[12] E. Ruckenstein, R. K. Jain, Spontaneous rupture of thin liquid films, Journal of the Chemical Society, Faraday Transactions 2: Molecular and Chemical Physics 70 (1974) 132–147.

[13] G. F. Teletzke, H. Ted Davis, L. E. Scriven, How liquids spread on solids, Chemical Engineering Communications 55 (1-6) (1987) 41–82.

[14] L. W. Schwartz, R. R. Eley, Simulation of droplet motion on low-energy and heterogeneous surfaces, Journal of Colloid and Interface Science 202 (1) (1998) 173–188.

[15] S. Jachalski, R. Huth, G. Kitavtsev, D. Peschka, B. Wagner, Stationary solutions of liquid two-layer thin-film models, SIAM Journal on Applied Mathematics 73 (3) (2013) 1183–1202.

[16] L. Giacomelli, H. Knüpfer, A free boundary problem of fourth order: classical solutions in weighted hölder spaces, Communications in Partial Differential Equations 35 (11) (2010) 2059–2091.

[17] J. Flitton, J. King, Surface-tension-driven dewetting of newtonian and power-law fluids, Journal of Engineering Mathematics 50 (2-3) (2004) 241–266.

[18] L. Giacomelli, M. V. Gnann, F. Otto, Regularity of source-type solutions to the thin-film equation with zero contact angle and mobility exponent between 3/2 and 3, European Journal of Applied Mathematics 24 (05) (2013) 735–760.

[19] G. Karapetsas, R. V. Craster, O. K. Matar, On surfactant-enhanced spreading and superspreading of liquid drops on solid surfaces, Journal of Fluid Mechanics 670 (2011) 5–37.

[20] R. Huth, S. Jachalski, G. Kitavtsev, D. Peschka, Gradient flow perspective on thin-film bilayer flows, Journal of Engineering Mathematics (2014) 1–19.

[21] G. Karapetsas, R. V. Craster, O. K. Matar, Surfactant-driven dynamics of liquid lenses, Physics of Fluids (1994-present) 23 (12) (2011) 122106.

[22] J. J. Kriegsmann, M. J. Miksis, Steady motion of a drop along a liquid interface, SIAM Journal on Applied Mathematics 64 (1) (2003) 18–40.

[23] T. Podgorski, J.-M. Flesselles, L. Limat, Corners, cusps, and pearls in running drops, Physical Review Letters 87 (3) (2001) 036102.